Effects of transducer size on impedance spectroscopy measurements

L. Mesin[1] and M. Scalerandi[2]
[1]*Department of Electronics and Telecommunications, Politecnico di Torino, Torino, Italy*
[2]*Department of Applied Science and Technology, Institute of Condensed Matter Physics and Complex Systems, Politecnico di Torino, Torino, Italy*
(Received 15 March 2012; published 21 May 2012)

The response to an electric field of electrolytic solutions, gels, liquid crystals, and other soft materials is described by the drift-diffusion and Poisson equations. Existing models, used for the interpretation of experimental data, usually consider the system as one dimensional (1D), which is valid only for an infinite electrode size. Here we solve numerically the model equations in 2D, considering a circular electrode with a finite radius, and discuss the limit of validity of the 1D approximation.

DOI: 10.1103/PhysRevE.85.051505 PACS number(s): 82.45.Fk, 84.37.+q, 82.45.Gj

I. INTRODUCTION

Electrolytic solutions, gels, liquid crystals, polymers, and other soft materials are physical systems sharing the characteristic of being composed of charged ions distributed in a liquid solution [1–4]. For their practical applications [5–7], it is important to understand their response to an external electric field and to estimate the physical properties of the impurity ions, such as density, charge, and diffusion coefficients. To this purpose, experimental methods have been developed to estimate the relaxation times of the system [8,9] and the impedance of an equivalent electric circuit, including the effects of the ionic redistribution when an external electric field is applied (impedance spectroscopy methods) [10–12].

In the latter case, two plane electrodes are applied to the system, confined in a given volume (cell). An external sinusoidal field (with varying frequency) is applied and the resulting electrical current in the circuit is measured. The system behaves approximately as an *RC* circuit, where the liquid is an insulating system and the mobile ions contribute to the ionic current in the cell. For low amplitudes of the applied potential and low density of the ions, the equivalent circuit behaves linearly. Thus, the system can be considered as a series of a resistance and a reactance, which are the real and imaginary parts of the impedance, respectively.

The interpretation of the results and the estimation of the ion parameters can then be obtained from models based on the drift-diffusion equation (describing the ionic redistribution) and the Poisson equation (describing the evolution of the electric field across the sample) [13–15]. In the one-dimensional (1D) limit, corresponding to an infinite electrode size, the solution of the problem can be analytically given, predicting (a) a resistance vanishing at high frequency (ω) and constant in the dc limit (low frequencies), and (b) a reactance which goes to zero (infinity) in the high (dc) limit, with a $1/\omega$ behavior in both limits. These predictions are not always verified in experimental conditions [16,17], thus posing questions about the adequacy of the models used.

Several explanations for the anomalous behavior of the experimental data can be found in the literature. Among them are ambipolar diffusion phenomena (due to ions with different mobilities) [18–20], anomalous diffusion (frequency dependent) [21,22], and non-perfectly-blocking electrodes [23–25]. Effects such as the existence of two plateaux in the resistance vs frequency curve or two minima in the reactance can be predicted. However, at least in some cases, the existing models cannot fully explain the impedance spectroscopy curves observed. Particularly critical is indeed the behavior of the reactance in the low frequency limit, which in some cases is not a $1/\omega$ behavior [26]. Whether these anomalous behaviors can be due to finite-size effects, such as those studied in electrochemical cells [27,28], is still an open question.

The goal of this paper is to analyze the effects of the finite size of the electrodes on the behavior of the system in order to understand whether this can explain some of the observed features. We will also study the importance of considering the electrode dimension when estimating the ionic parameters from impedance spectroscopy measurements. In the next section, the physical equations governing the problem are briefly recalled and the numerical implementation is discussed. Results will be presented in Sec. III and the importance of our findings for practical applications will be discussed in Sec. IV.

II. THEORY

A. The physical problem

Let us consider an electrolytic cell containing an ionic solution, where positive and negative ions are both mobile ($D_\pm$ being the respective diffusion coefficients). For simplicity, we neglect dissociation and recombination phenomena during the evolution of the system. At the initial time, the sample is locally neutral and ions are uniformly distributed, with density n_0 (the same for positive and negative ions). Ions have a charge q. The liquid in which ions are dispersed is defined by a dielectric constant ε. The electrolytic cell is considered as a cylinder with radius L and length d; see Fig. 1. The coordinate system is oriented with the z axes parallel to the length of the cylinder ($-d/2 \leqslant z \leqslant d/2$). Two plane circular electrodes (of radius $r < L$) are placed on the top and bottom surfaces of the cell. The electrodes are connected to an external circuit supporting a potential applied to the cell in the form $\Delta V_{\text{ext}} = A \exp(j\omega t)$. Here, the amplitude A is considered small, as in experiments, and it is not a relevant parameter. ω is the angular frequency.

As soon as the external potential is applied, the electric field generated in the sample causes a redistribution of ions (although the sample remains globally neutral), which in turn generates an additional electric field. We can define a vectorial

drift-diffusion current (for positive and negative ions) as

$$\mathbf{j}_\pm = -D_\pm \nabla n_\pm \mp \mu_\pm n_\pm \nabla V, \tag{1}$$

where $\mu_\pm = qD_\pm/K_BT$ is the ionic mobility (K_B is the Boltzman constant and T is the absolute temperature). The following evolution equations for the ionic bulk densities $n_\pm(x,y,z,t)$ and the potential $V(x,y,z,t)$ across the sample can thus be written as

$$\frac{\partial n_\pm}{\partial t} = -\nabla \cdot \mathbf{j}_\pm, \quad \nabla^2 V = -\frac{q}{\varepsilon}(n_+ - n_-). \tag{2}$$

The second is the Poisson equation.

Boundary conditions are defined as a vanishing normal current $j_\pm^{\mathbf{N}}$ along each border of the cell,

$$j_\pm^{\mathbf{N}} = 0, \tag{3}$$

for $z = \pm d/2$ and for $\rho = \sqrt{x^2+y^2} = L$. Boundary conditions for the potential indicates that an external voltage V_{ext} is applied on the electrodes surfaces ($z = \pm d/2$ and $\rho \leqslant r$). The continuity of the normal component of the dielectric displacement vector $\mathbf{D} = \varepsilon\mathbf{E}$ between the inside and outside of the cell is forced on the other boundaries ($\mathbf{E}$ is the electric field).

In cylindrical coordinates, and given the symmetry of the system for rotations (i.e., variables do not depend on the angle), Eqs. (2) can be rewritten as

$$\frac{\partial n_\pm}{\partial t} = D_\pm\left[\frac{\partial^2 n_\pm}{\partial z^2} + \frac{1}{\rho}\frac{\partial}{\partial \rho}\left(\rho\frac{\partial n_\pm}{\partial \rho}\right)\right] \mp \mu_\pm n_\pm\left[\frac{\partial^2 V}{\partial z^2} + \frac{1}{\rho}\frac{\partial}{\partial \rho}\left(\rho\frac{\partial V}{\partial \rho}\right)\right]$$
$$\left[\frac{\partial^2 V}{\partial z^2} + \frac{1}{\rho}\frac{\partial}{\partial \rho}\left(\rho\frac{\partial V}{\partial \rho}\right)\right] = -\frac{q}{\varepsilon}(n_+ - n_-). \tag{4}$$

Furthermore, if the amplitude A of the potential applied to the cell is sufficiently small, as in a large number of applications [29], then nonlinear terms can be neglected. In particular, introducing the local change in ionic density $\delta n_\pm(r,z) = n_\pm(r,z) - n_0$, we have $\delta n_\pm(r,z) \ll n_0$. Substituting in Eq. (4) and neglecting higher order terms, we get

$$\frac{\partial(\delta n_\pm)}{\partial t} = D_\pm\left[\frac{\partial^2(\delta n_\pm)}{\partial z^2} + \frac{1}{\rho}\frac{\partial}{\partial \rho}\left(\rho\frac{\partial(\delta n_\pm)}{\partial \rho}\right)\right] \mp \mu_\pm n_o\left[\frac{\partial^2 V}{\partial z^2} + \frac{1}{\rho}\frac{\partial}{\partial \rho}\left(\rho\frac{\partial V}{\partial \rho}\right)\right]$$
$$\left[\frac{\partial^2 V}{\partial z^2} + \frac{1}{\rho}\frac{\partial}{\partial \rho}\left(\rho\frac{\partial V}{\partial \rho}\right)\right] = -\frac{q}{\varepsilon}(\delta n_+ - \delta n_-). \tag{5}$$

The boundary conditions in cylindrical coordinates are

$$V(\rho \leqslant r, z = \pm d/2) = A\exp(j\omega t),$$
$$\frac{\partial V}{\partial z}(\rho > r, z = \pm d/2) = 0, \tag{6}$$

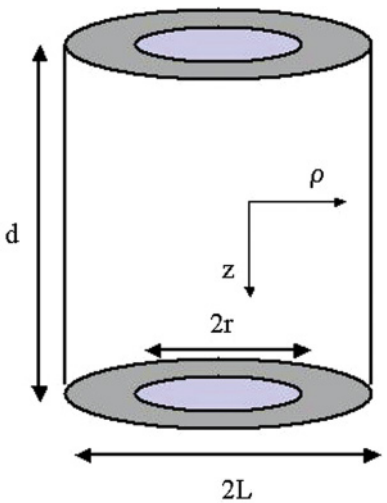

FIG. 1. (Color online) Schematic representation of the cell configuration.

$$j_\pm^N(\rho, z = \pm d/2) = \mathbf{j}_\pm(\rho = \pm L, z = \pm d/2)\cdot\mathbf{N} = 0,$$
$$\frac{\partial V}{\partial \rho}(\rho = \pm L, z) = 0. \tag{7}$$

Note that the second and last boundary conditions (equivalent to homogeneous Neumann conditions) are valid when the dielectric constant of the cell is large (compared to that of air) and when L is sufficiently larger than the transducer radius r, respectively. Both conditions are normally verified in practical cases (and in our simulations). Otherwise, continuity of the normal component of the dielectric displacement vector $\mathbf{D} = \varepsilon\mathbf{E}$ should be imposed.

The problem is thus a 2D linear system of equations which, as we will see in the next section, can be solved numerically. However, before moving on, we remind the reader that in the case of plane electrodes with infinite extension, we also have a symmetry in the radial direction. Thus the system becomes 1D and it is possible to derive an analytical solution (not discussed here for brevity) [14].

B. Numerical solution

To numerically solve the problem, we observe that since the model equations are linear, we can write

$$V = \hat{V}e^{j\omega t}, \quad \delta n_\pm = \delta\hat{n}_\pm e^{j\omega t}.$$

Therefore, time derivatives can be replaced by multiplication for $j\omega$. Thus the problem is reduced to find the solution in the space domain of the linear system of complex equations:

$$j\omega\delta\hat{n}_{\pm} = D_{\pm}\left\{\frac{\partial^2(\delta\hat{n}_{\pm})}{\partial z^2} + \frac{1}{\rho}\frac{\partial}{\partial\rho}\left[\rho\frac{\partial(\delta\hat{n}_{\pm})}{\partial\rho}\right]\right\} \mp \mu_{\pm}n_o\left[\frac{\partial^2\hat{V}}{\partial z^2} + \frac{1}{\rho}\frac{\partial}{\partial\rho}\left(\rho\frac{\partial\hat{V}}{\partial\rho}\right)\right]$$

$$\left[\frac{\partial^2\hat{V}}{\partial z^2} + \frac{1}{\rho}\frac{\partial}{\partial\rho}\left(\rho\frac{\partial\hat{V}}{\partial\rho}\right)\right] = -\frac{q}{\varepsilon}(\delta\hat{n}_{+} - \delta\hat{n}_{-}). \tag{8}$$

We defined a bounded space domain, imposing a maximum radius L, where homogeneous Neumann boundary conditions were assumed for the potential ($\frac{\partial\hat{V}}{\partial\rho} = 0$) and no flux conditions were imposed for the ion densities. A maximum radius r for the electrodes was also chosen so that the electric field and the variation of the ion densities close to the cell boundary ($\rho = L$) were negligible. The mathematical problem was solved using the finite difference method [30]. A nonuniform discretization of the domain was used, with increasing resolution close to the electrodes, particularly near the edges. The increased resolution area covered a distance a few debye lengths from the electrode (both in the z direction and from the edges). First- and second-order space derivatives were discretized with a second-order approximation, both within the domain and on the boundary. For the first derivative, we have

$$\left.\frac{\partial u}{\partial x}\right|_{x_0} \cong au(x_0) + bu(x_0 + h_1) + cu(x_0 + h_2), \tag{9}$$

where $a = -\frac{h_1+h_2}{h_1h_2}$, $b = -\frac{h_2}{h_1(h_1-h_2)}$, and $c = \frac{h_1}{h_2(h_1-h_2)}$, and for the second derivative, we have

$$\left.\frac{\partial^2 u}{\partial x^2}\right|_{x_0} \cong au(x_0) + bu(x_0 + h_1) + cu(x_0 + h_2), \tag{10}$$

where $a = \frac{2}{h_1h_2}$, $b = \frac{2}{h_1(h_1-h_2)}$, and $c = -\frac{2}{h_2(h_1-h_2)}$. Notice that h_1 and h_2 have the same sign when the considered point x_0 is on the boundary and different signs when x_0 is within the domain.

Using discretization of derivatives, the problem is reduced to a linear system of algebraic equations, which allows calculation (in the complex space) of the spatial distributions of the ion densities and the potential for any frequency: $\delta n_{\pm}(\rho,z,\omega)$ and $V(\rho,z,\omega)$. The solution was estimated resolving such a system using the Gauss elimination method. Multiplication by $e^{j\omega t}$ brings the solutions back into the time domain.

Given the potential, the charge Q over one electrode (which is the same, except for the sign, as that over the other electrode) was estimated, using the integral form of Gauss's law, as

$$Q(\omega) = \left[\int_{\rho\leqslant r,\, z=d/2} \mathbf{D}\cdot\mathbf{N}dS\right] = 2\pi\varepsilon\int_0^r \rho\frac{\partial V}{\partial\rho}d\rho, \tag{11}$$

where $\mathbf{N}$ is the versor normal to the electrode.

The current flowing through the electrode was obtained by a time derivative of the charge (i.e., a multiplication by $j\omega$). From the estimated current and the imposed potential, the impedance was computed in the complex domain as

$$Z = \frac{A}{j\omega Q}. \tag{12}$$

The independence of the solution from the discretization steps and from the discrete integration method has been carefully verified.

The methods were implemented in MATLAB, on a Pentium(R) Dual-Core computer, with clock frequency of 2.8 GHz, 4 GB of RAM, and 64-bit operating system, using routines running on a single core. The average computational time for a single simulation (which means a single cell, with a specific radius of the electrode, considering a single frequency of the voltage source) was about 60 s (with about 30 s of variation between the fastest and the slowest simulation).

The spatial sampling of the cell depended on the radius of the electrode and on the frequency. The maximum sampling interval of the radial variable far from the electrode was about 3 mm; the sampling spacing in the center of the electrode was one-hundredth of the electrode radius; the minimum spacing between sample points was close to the electrode circumference, where it was equal to the minimum value between one-twentieth of the sampling interval in the center of the electrode and one-fourth of the minimum eigenvalue of the linearized system of equations (which depended on debye length and frequency). The maximum sampling interval of the z variable was about 66 μm; the minimum spacing between sample points was close to the electrode, where it was equal to the minimum value between one-twentieth of the maximum sampling interval of the z variable and one-fourth of the minimum eigenvalue of the linearized system of equations. The sampling steps were smoothly varied between the different extremes detailed above. The resulting sampling of the radial coordinate was constituted by about 250 points, whereas the z variable was sampled using about 150 points.

C. Analysis of impedance spectroscopy data

As mentioned in the previous section, numerical simulations allow the calculation of the potential and the densities of ions for any frequency of the external potential and any position in the sample. In particular, it is possible to calculate the charge on the electrode needed to support the external potential [Eq. (11)] and the cell impedance Z [see Eq. (12)]. The above equation allows computation of the resistance [$R = \mathrm{Re}(Z)$] and reactance [$X = \mathrm{Im}(Z)$] of the equivalent circuit of the electrolytic cell.

As mentioned before, in the 1D case an analytical solution can be given for the ion distribution. Thus the impedance can

be exactly calculated. It results in

$$Z_{1D} = -i\frac{2}{\omega\varepsilon\pi r^2\beta^2}\left\{\frac{1}{\lambda^2\beta}\tanh(\beta d/2) + i\frac{\omega d}{2D}\right\},$$
$$\beta^2 = \frac{1}{\lambda^2}\left(1 + i\frac{\omega}{D}\lambda^2\right), \quad \lambda^2 = \frac{\varepsilon k_B T}{2N_0 q^2}. \tag{13}$$

Details of the derivation are reported in Ref. [14].

It is interesting to observe that in the $\omega \to \infty$ limit, ions do not participate in the dynamics of the system. Since the electric fields vary very rapidly, the relaxation times are longer than the electric field period and ions could be considered as fixed. It follows that the cell behaves as a perfect capacitor bounded by finite circular electrodes. In this case, resistance goes to zero and the cell reactance diverges linearly with the frequency.

III. RESULTS

Simulations have been performed using the approach discussed above to analyze the frequency dependence of the resistance and reactance of the electrolytic cell, which was considered as a cylinder with length $d = 2$ mm and radius $L = 100$ mm. The radius of the electrode varied between $r = 0.5$ and 80 mm. Parameters used in the simulations are $n_0 = 10^{22}$ ions per m^3, $D_+ = D_- = 2 \times 10^{-9}$ m^2/s, $\varepsilon = 80$, q is the charge of a proton, and $T = 300$ K. The frequency is varied in the range $10^{-3} < f = \frac{\omega}{2\pi} < 10^7$ Hz. The amplitude of the external potential is fixed to 1 mV; due to the linearity of the system (in the amplitude range considered), this is not a relevant parameter.

A. Impedance spectroscopy

In Fig. 2, R and $-X$ are plotted vs frequency for the smallest and largest considered radius of the electrode (upper row: $r = 0.5$ mm; lower row: $r = 80$ mm). In both cases, the numerical solution (dashed red line) is compared to the analytical one [see Eq. (13)] in the case of an infinite electrode (solid blue line), which from now on will be called the 1D limit. As expected, the analytical solution is valid only when $r \gg d$; otherwise, the 1D solution is inadequate.

To better analyze the effects of the finite size of the electrodes, in Fig. 3 the resistance and reactance are plotted vs the frequency for a few selected radii of the electrodes. The numerical solution converges to the analytical one (solid black line) when r increases. However, significant differences from the 1D limit are already evident for $r = 20$ mm (i.e.,

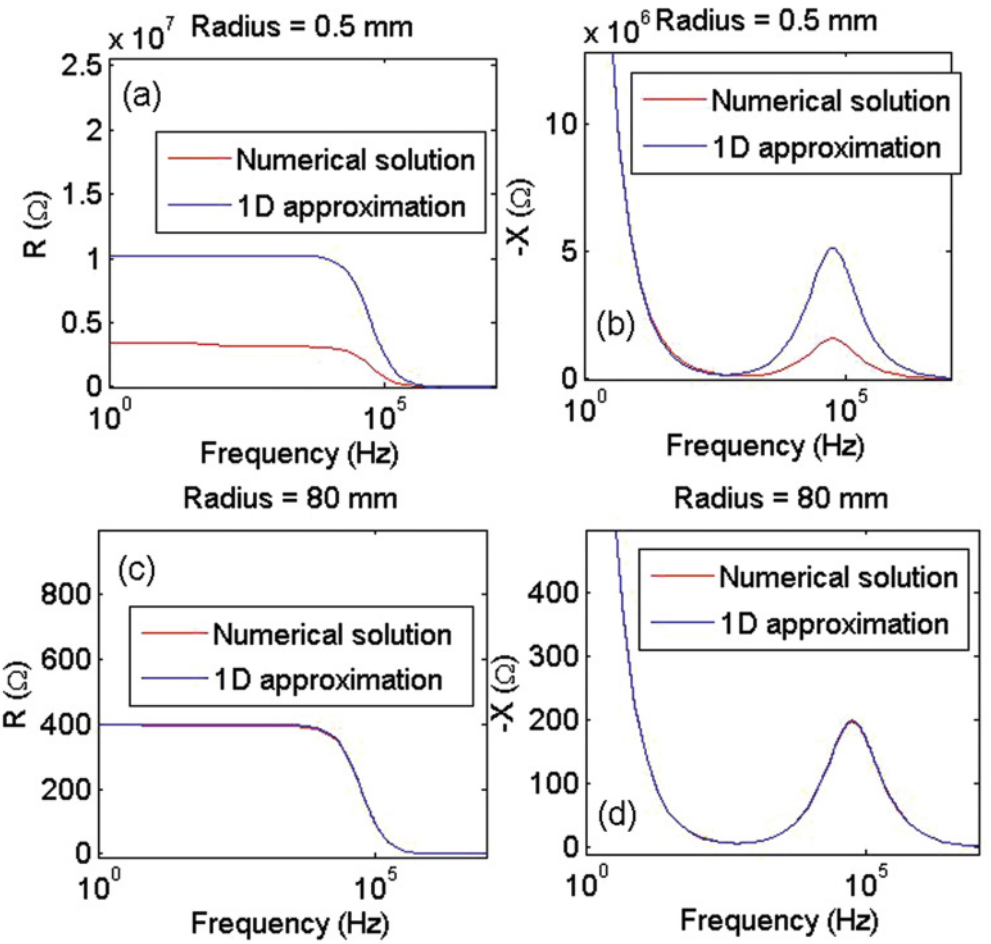

FIG. 2. (Color online) Real (R) and imaginary ($-X$) parts of the cell impedance vs frequency for a small and large radius of the electrode (0.5 and 80 mm, respectively) in the upper and lower row, respectively. The numerical solution (dashed red line) is compared with the 1D limit (solid blue line).

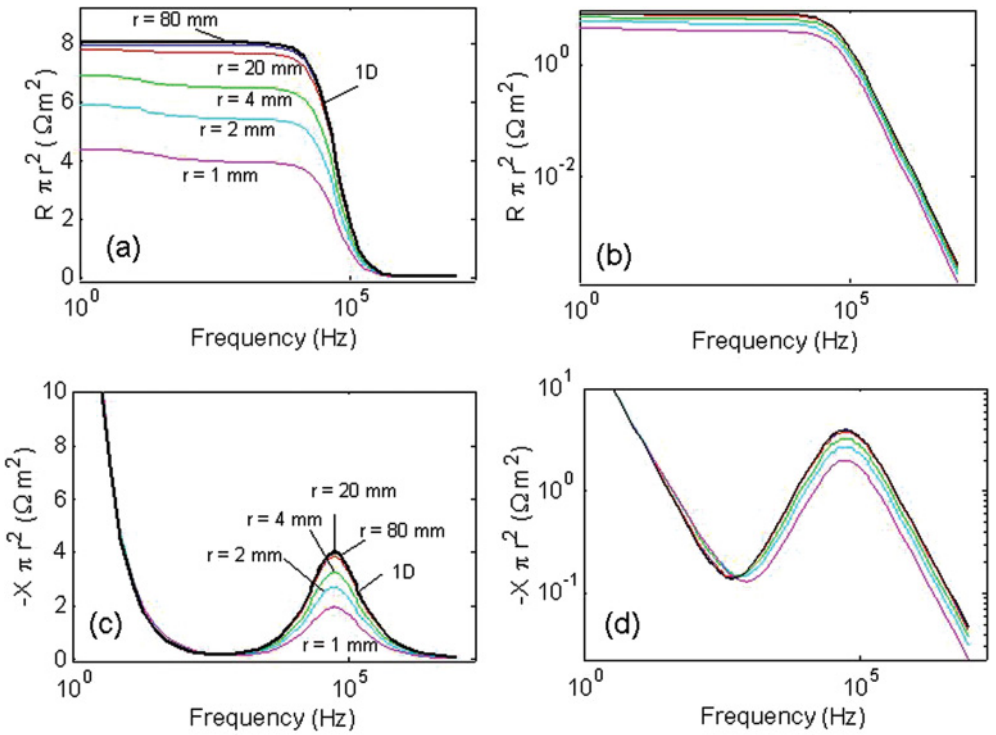

FIG. 3. (Color online) Real (R) and imaginary ($-X$) parts of the cell impedance (multiplied by the electrode section πr^2) vs frequency for different radii of the electrode: $r = 80$ mm (blue line); $r = 20$ mm (red line); $r = 4$ mm (green line); $r = 2$ mm (cyan line); $r = 1$ mm (magenta line); 1D limit (black line). (a), (b) Resistance in semilog and log-log scales, respectively. (c), (d) Reactance in semilog and log-log scales, respectively.

$r/d = 10$), for cases of interest in experimental studies. The electrode finite-size effects detectable in Fig. 3 are as follows:

(i) The dc limit of the resistance per unit surface $R\pi r^2$ decreases with r and the plateaux is split into two regions [Figs. 2 and 3(a)] . In particular, the ratio between the resistance found in numerical experiments and the 1D limit findings is always smaller than one (the 1D limit overestimates the resistance in dc).

(ii) The maximum of the reactance at intermediate frequencies ($\omega \sim 10^5$) increases with r [see Fig. 3(c)] and distortions of the curve are present around the minimum of the reactance [Fig. 3(d)].

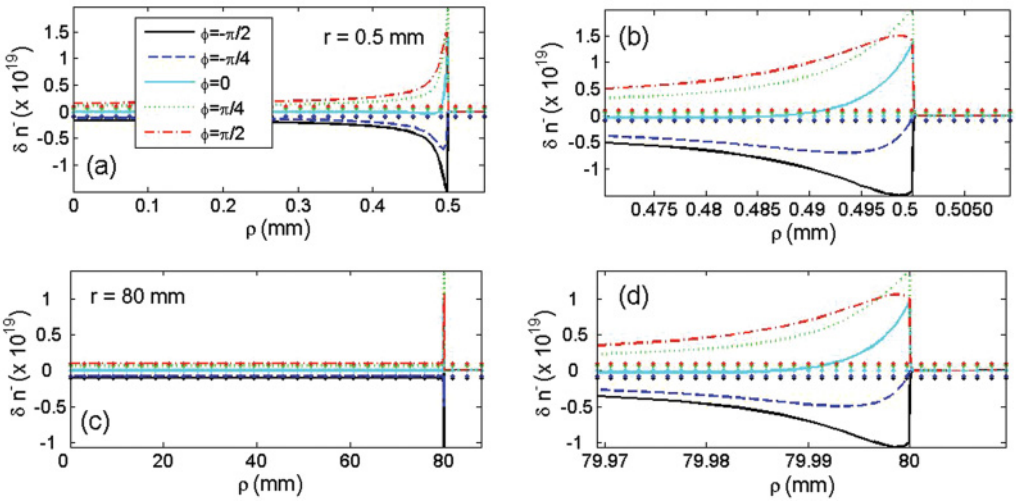

FIG. 4. (Color online) Distribution of $\delta n^-(z = d/2, \rho)$ vs the radial coordinate for a small and large radius of the electrode. Different colors correspond to different phases, i.e., to different times during the evolution. The analytical limits are plotted as dotted lines (and of course are independent from ρ). (a), (c) Distribution in the range $0 \leqslant \rho \leqslant 1.1r$. (b), (d) Zoom of (a) and (c) around the electrode edge ($r - 0.03$ mm $\leqslant \rho \leqslant r + 0.01$ mm). The left column shows that for a large radius, the edge effects are negligible, while the right column shows the different characteristic decay scales in the inward and outward (from edge) directions.

(iii) The resistance in the high frequency limit goes to zero as ω^{-2}, as in the 1D limit [Fig. 3(b)].

(iv) In both the low and high frequency limits, the reactance behaves as $1/\omega$, as in the 1D limit [Fig. 3(d)].

All such effects will be quantified in the next section and their implications discussed.

B. Spatial distribution close to electrodes

To understand the origin of the finite-size effects observed, we investigate in Fig. 4 the time evolution of the spatial distribution in front of the electrode of negative ions for a fixed frequency ($\omega = 828$ Hz, corresponding to the second plateaux) and a small and large radius ($r = 0.5$ mm and $r = 80$ mm, respectively). In both cases, the distribution at different time instances within one period are reported with different colors and line types. We recall that different times correspond to different phases. It is to be noted that the distribution follows, with some delay, the applied potential [$V(z = -d/2) = -A\sin(\Phi)$]. The solution converges to the 1D limit (reported with circles) at $\rho = 0$ (center of the electrode) for both radii [Figs. 4(a) and 4(c)], and 2D effects are limited in a small area at the electrode edges ($\rho = r$). Zooming around the edge [Figs. 4(b) and 4(d)], the behavior for the two radii looks very similar, as will be better discussed in the following. However, it is evident that the 2D effects on the charge accumulated on the electrode are negligible only for a large electrode radius. In fact, the affected region has the same spatial size (of the order of ten μm) for both radii.

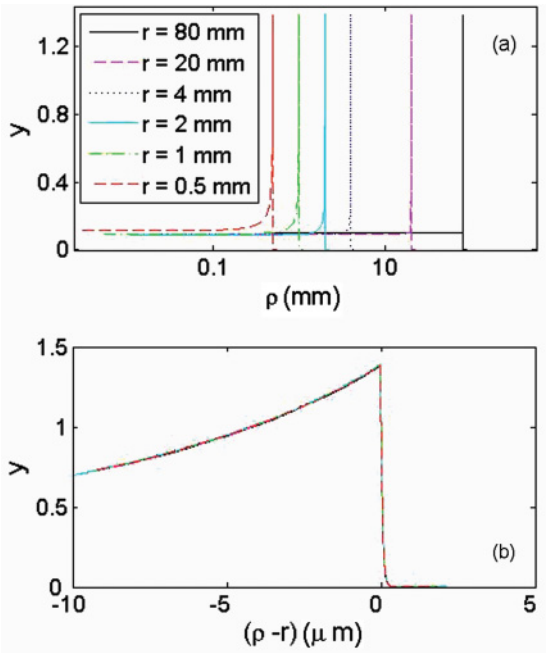

FIG. 5. (Color online) (a) Variation in ion density normalized through the function defined in Eq. (14) vs ρ. (b) Variation in ion density normalized through the function defined in Eq. (14) vs $\rho - r$. Curves corresponding to all radii (from 0.5 to 80 mm) scale onto a single curve.

To verify the scaling properties of the ion distributions with varying r, it has been found that ions profiles in front of the electrode scale in a single curve when normalized through the function:

$$f(r) = a + b/r. \tag{14}$$

For the case considered in Fig. 4, it has been found that $a = 1$ and $b = 2.1 \times 10^{-4}$ m. Plots of

$$y = \frac{\delta n_{-}(-d/2, \rho)}{f(r)} \tag{15}$$

for various radii are reported in Figs. 5 (y vs ρ for $z = -d/2$) and 5(b) (y vs $\rho - r$). Here we considered $\Phi = \pi/2$. The curves corresponding to different radii scale in a single curve remarkably well. An extensive analysis has been performed and has proven that b is independent from n_0 and from the frequency (except at very low frequencies where the differences after scaling are significant).

In Fig. 6, we analyze the behavior of the ion distribution close to the electrode edges for different frequencies (for $\Phi = \pi/2$). We consider a radius of $r = 2$ mm. The plot in Fig. 6(a) (resistance vs frequency) shows that the chosen frequencies correspond to the two resistance plateaux, to the inflection points in the R vs ω curve, and to a high frequency. The other subplots show the distribution of negative ions (close to the electrode edge) normalized to its value at the electrode

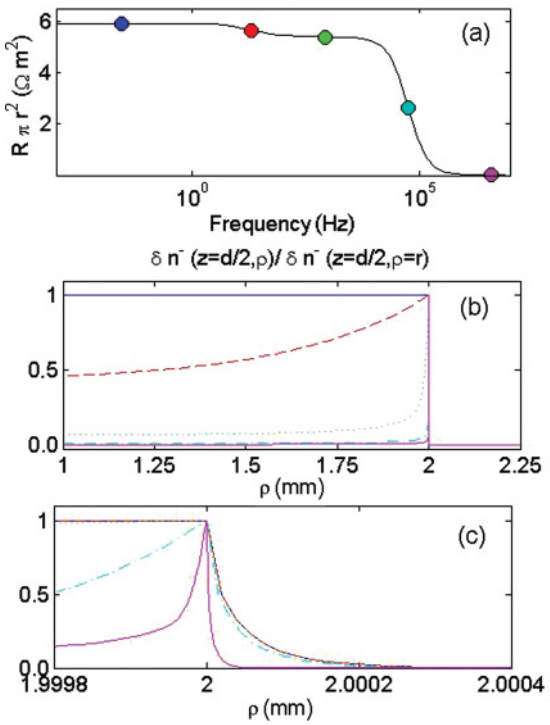

FIG. 6. (Color online) Modulus of the variation in ion density $\delta n^{-} = n^{-} - n_0$ for some frequencies of the applied electric field in front of the electrode. (a) The real part R of the cell impedance (multiplied by the electrode section πr^2) is shown as a function of frequency for the radius of the electrode, $r = 2$ mm. Five values of frequency are indicated and considered for the other plots as follows: on the first plateau, on the first inflection point, on the second plateau, on the last inflection point, and at high frequency. (b) δn^{-} normalized to its value for $z = d/2, \rho = r$. (c) Zoom of (b) around the electrode edge.

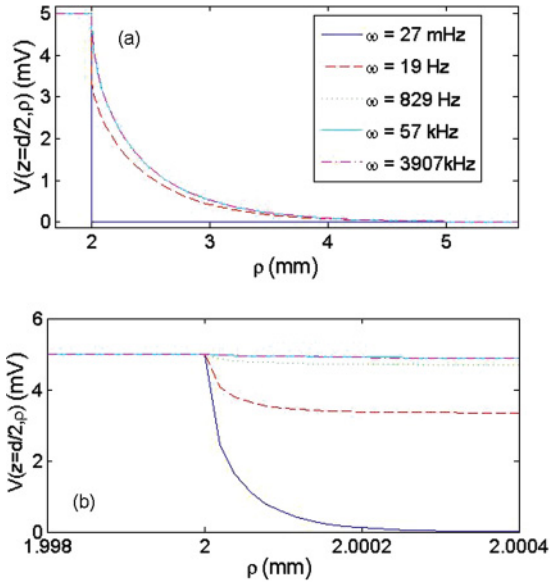

FIG. 7. (Color online) (a) Potential V at $z = d/2$ (in front of the electrode surface) as a function of ρ. (b) Zoom of (a) around the electrode edge. Same case as Fig. 6.

edge. We can observe that the ionic density at the edge of the electrode ($\rho = r, z = d/2$) is very different from the expected 1D limit [Fig. 6(b)]. Furthermore, it has a different decay in the inward and outward directions. In particular, δn_- decays rapidly to zero from the edge of the electrode outward, within a typical length of the order of that of debye [Fig. 6(c)]. Decay is much faster at higher frequencies (as expected). The decay length is much higher in the inward direction (from edge to center), again significantly increasing for decreasing frequency.

As a consequence of the redistribution of ions, the potential decays rapidly from the edge of the electrode [Fig. 7(a)], becoming negligible within a few mm distance from the edge. In addition to this effect, typical of a finite-size condenser, a decay can be appreciated on a smaller length scale (that of the debye length). The effect can be appreciated when zooming around $\rho = r$ [Fig. 7(b)], where the apparent jump of potential immediately close to the edge of the electrode visible in Fig. 7 is indeed shown to be a fast decay. The effect is more significant at low frequency (blue line) and almost negligible at high frequency (magenta line).

Similar considerations hold true for the distribution of δn^- as a function of z (not reported for brevity). The solution at $\rho = 0$ is the same as for the 1D limit for both a large and small radius. On the contrary, huge differences from the analytical solution are present for $\rho = r$. In both cases, the distribution decays to zero in a region of the order of the debye length from the electrode edge inward.

IV. DISCUSSION

To quantify effects due to the finite size of the electrodes, we consider here the major features in the resistance and reactance vs frequency curves.

Considering the reactance $-X$, as mentioned, the more meaningful features are the position of the maximum and minimum (see Fig. 2). In Fig. 8(a), $-X\pi r^2$ vs ω is plotted around $\omega = \omega_{1D}^{max}$ (where ω_{1D}^{max} is the frequency corresponding to the position of the maximum in the 1D limit). It can be seen that the frequency ω^{max} corresponding to the maximum of the reactance does not depend on the electrode radius [Fig. 8(b)], while $-X(\omega_{1D}^{max})$ increases with r up to saturating to the value assumed in the 1D approximation [Fig. 8(c)]. Different is the case of the minimum of $-X\pi r^2$ [plotted in Fig. 9 vs frequency around the frequency corresponding to the minimum position in the 1D approximation]. Here, the frequency diminishes with increasing radius, up to saturating at the 1D approximation value. The value of $-X\pi r^2$ in correspondence to the minimum, first increases then decreases with increasing r (again saturating towards the 1D limit).

Finally, in Fig. 10, the dc limit of the resistance $R\pi r^2$ and the position of the three inflection points are studied as functions of the radius of the electrode. In Fig. 10(a), $R\pi r^2$ is plotted vs frequency and the inflection points for each curve are reported as squares or red circles. Also, the plateaux values are identified with triangles and red squares. The positions

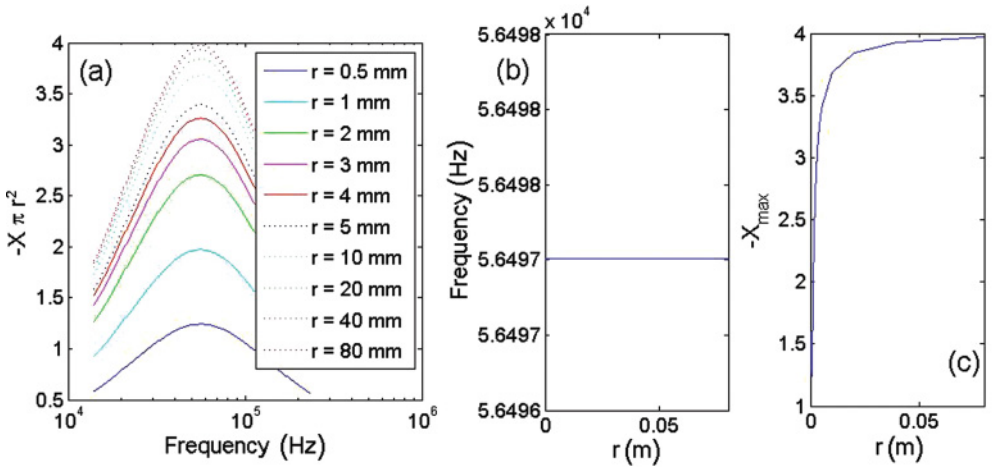

FIG. 8. (Color online) (a) Behavior of the reactance ($-X\pi r^2$) vs frequency around the position of its maximum (see Fig. 1 for the full curve). (b) Position of the maximum of (a) vs the electrode radius. (c) Amplitude of the maximum of (a) vs the electrode radius.

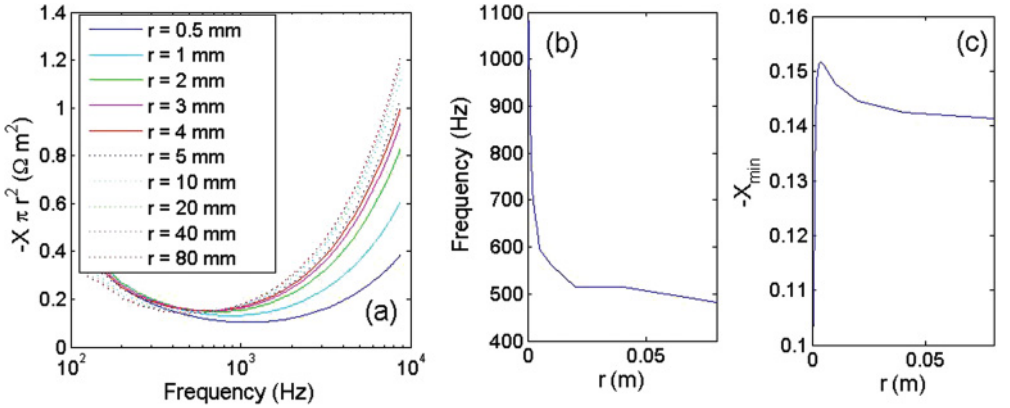

FIG. 9. (Color online) (a) Behavior of the reactance $(-X\pi r^2)$ vs frequency around the position of its minimum (see Fig. 1 for the full curve). (b) Position of the minimum of (a) vs the electrode radius. (c) Amplitude of the minimum of (a) vs the electrode radius.

of the three inflection points as functions of the radius are shown in Fig. 10(b). The inflection point at large frequency does not change with r and corresponds to the inflection point found in the 1D limit. The other two inflection points move to lower frequencies increasing r and disappear in the $r \to \infty$ limit. The difference of the resistance values at the two plateaux are reported vs r in Fig. 10(c). It converges to zero for large values of the electrode radius and presents a maximum when the frequency is decreased. Finally, in Fig. 10(d), the resistance in the dc limit $(R\pi r^2)$ is plotted vs the electrode radius. As expected, the resistance increases with increasing r and converges to the 1D limit, thus indicating the presence

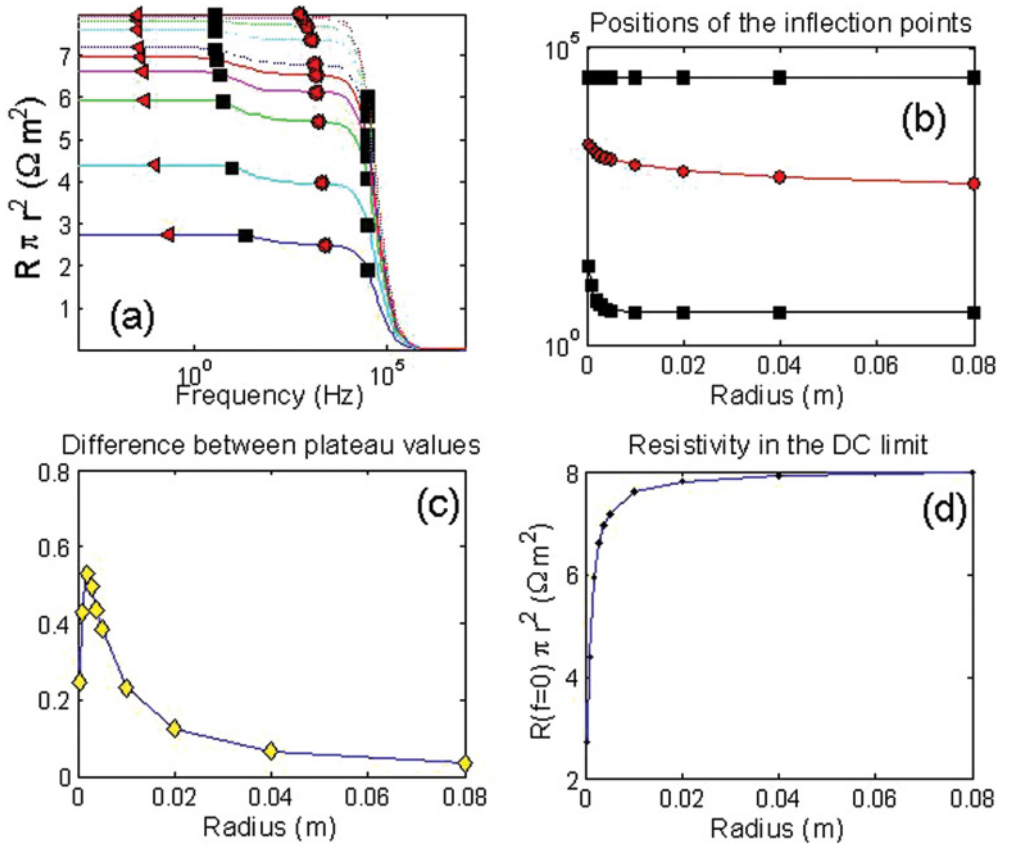

FIG. 10. (Color online) (a) Behavior of the resistance $R\pi r^2$ as a function of frequency. Three inflection points (black squares and red circles) can be identified for each curve. Also two plateaux values of the resistance (red triangles and circles) are visible. (b) Position of the three inflection points vs radius of the electrode. (c) Difference between plateaux values of resistance as a function of the electrode radius. (d) Behavior of the resistance $R\pi r^2$ as a function of the electrode radius in the dc limit.

of an additional electric current due to finite-size effects at the electrode edges.

V. CONCLUSIONS

In this paper, we analyzed the effects on the ion redistribution in an electrolytic cell (and affine systems) due to the finite size of the electrodes used to apply an electrical potential. In particular, we studied the variations of the frequency dependence of the resistance and reactance of the system (impedance spectroscopy experiments).

We found that such effects are not negligible already when the electrode radius is of the order of $10d$ (where d is the distance between the electrodes), i.e., in common experimental situations. The major effects observed are the appearance of two plateaux in the resistance, the reduction of the resistance in the dc limit, and a variation in the frequency of the minimum of the reactance. We also showed that such effects are due to local variations in the ionic distribution localized in a very narrow region at the edges of the electrodes. Such effects (due to their localization) do not seem to be removed when introducing a guard ring.

Thus, particular care has to be used when applying the solution of 1D models of the electrolytic cell to estimate the ionic parameters, such as concentration and diffusion coefficients. The results presented here indicate that 2D effects (in cylindrical coordinates) might be responsible for some of the anomalous effects observed in experiments (such as the two plateaux resistance behavior). However, other effects cannot be simply ascribed to the finite size of the electrodes. Among them, in experiments [16], a decay of the reactance in the dc limit is often observed that is not proportional to $1/\omega$. Our findings indicate that in the dc (and high frequency) limits, the behavior of reactance still remains as in the 1D limit ($1/\omega$ for both high and dc limits of the reactance). Thus other causes have to be individuated to explain such a set of experimental data.

Further studies will be devoted to consider finite-size effects due to the transducer when more complex systems are considered. Among them, equations will be modified to include more than one ion species, adsorption effects, and frequency-dependent diffusion (or dielectric constant) parameters. Such physical mechanisms alone (ambipolar diffusion, double layer effects, etc.) have proven to be insufficient to explain completely the anomalous behaviors in the experimental data discussed above. However, their combination with the transducer size effects discussed here might provide a satisfactory interpretation of the measured impedance of systems such as gels for biomedical applications (work in progress).

ACKNOWLEDGMENT

We thank G. Barbero (Politecnico di Torino) for useful discussions and support.

[1] T. L. Lasseter, W. Cai, and R. J. Hamers, Analyst **129**, 38 (2004).
[2] A. Mazzulla, F. Ciuchi, and R. Sambles, Phys. Rev. E **64**, 021708 (2001).
[3] H. Zhao, Phys. Rev. E **84**, 051504 (2011).
[4] F. Bougrioua, H. De Vleeschouwer, S. Vermael, K. Neyts, and H. Pauwels, Mol. Cryst. Liq. Cryst. **367**, 45 (2001).
[5] W. Xiao and H. Wei, Phys. Rev. E **81**, 041803 (2010).
[6] R. Aamir *et al.*, PloS ONE **6**, 0029243 (2011).
[7] M. Felkzac and G. Derfel, Liq. Cryst. **30**, 739 (2003).
[8] M. Z. Bazant, K. Thornton, and A. Adjadari, Phys. Rev. E **70**, 021505 (2004).
[9] F. C. M. Freire, A. Alexe-Ionescu, M. Scalerandi, and G. Barbero, Appl. Phys. Lett. **89**, 214101 (2006).
[10] A. Mazzulla, F. Ciuchi, and R. Sambles, Phys. Rev. E **68**, 023702 (2002).
[11] M. Becchi, C. Avendano, A. Strigazzi, and G. Barbero, J. Phys. Chem. B **109**, 23444 (2005).
[12] P. A. Cirkel, J. P. M. van der Ploeg, and G. J. M. Koper, Physica A **235**, 269 (1997).
[13] J. Ross Macdonald, J. Phys. Chem. A **115**, 13370 (2011).
[14] I. Lelidis and G. Barbero, Phys. Lett. A **343**, 440 (2005).
[15] G. Barbero and M. Scalerandi, J. Chem. Phys. **136**, 712 (2012).
[16] A. L. Alexe-Ionescu, G. Barbero, F. C. M. Freire, and R. Merletti, Physiol. Meas. **31**, S169 (2010).
[17] L. F. Marchesi, F. R. Simoes, L. A. Pocrifka *et al.*, J. Phys. Chem. B **115**, 9570 (2011).
[18] A. L. Alexe-Ionescu, G. Barbero, I. Lelidis, and M. Scalerandi, J. Phys. Chem. B **111**, 13287 (2007).
[19] G. Sandip and C. Zhen, Proc. R. Soc. London A **466**, 2145 (2010).
[20] G. Barbero and I. Lelidis, Phys. Rev. E **76**, 051501 (2007).
[21] E. K. Lenzi *et al.*, Phys. Rev. E **84**, 041128 (2011).
[22] L. R. Evangelista *et al.*, J. Phys. Condens. Matter **23**, 485005 (2011).
[23] H. Chang and G. Jaffe, J. Chem. Phys. **20**, 1071 (1952).
[24] G. Barbero, F. Batalioto, and A. M. Figueiredo Neto, J. Appl. Phys. **101**, 054102 (2007).
[25] J. R. Madonald, J. Phys. D: Condens. Matter **22**, 495101 (2010).
[26] G. Barbero, M. Becchi, and F. C. M. Freire, J. Appl. Phys. **104**, 114111 (2008).
[27] C. Gabrielli *et al.*, J. Phys. Chem. B **110**, 20478 (2006).
[28] M. Cimenti, V. I. Birss, and J. M. Hill, Fuel Cells **7**, 377 (2007).
[29] F. C. M. Freire, G. Barbero, and M. Scalerandi, Phys. Rev. E **73**, 051202 (2006).
[30] R. J. LeVeque, *Finite Difference Methods for Ordinary and Partial Differential Equations* (SIAM, Philadelphia, 2007)